

# Sustainable Food Technology

Accepted Manuscript

This article can be cited before page numbers have been issued, to do this please use: S. Xiao, B. Chen, J. Yu, H. Hu, Y. Wang, X. Sun, H. Li and H. Li, *Sustainable Food Technol.*, 2026, DOI: 10.1039/D6FB00033A.



This is an Accepted Manuscript, which has been through the Royal Society of Chemistry peer review process and has been accepted for publication.

Accepted Manuscripts are published online shortly after acceptance, before technical editing, formatting and proof reading. Using this free service, authors can make their results available to the community, in citable form, before we publish the edited article. We will replace this Accepted Manuscript with the edited and formatted Advance Article as soon as it is available.

You can find more information about Accepted Manuscripts in the [Information for Authors](#).

Please note that technical editing may introduce minor changes to the text and/or graphics, which may alter content. The journal's standard [Terms & Conditions](#) and the [Ethical guidelines](#) still apply. In no event shall the Royal Society of Chemistry be held responsible for any errors or omissions in this Accepted Manuscript or any consequences arising from the use of any information it contains.

## Sustainability spotlight

This study supports sustainability by constructing a pH-responsive fucoidan/carboxymethyl chitosan hydrogel beads for the encapsulation of bioactive curcumin. An innovative and environmentally friendly strategy was developed for the fabrication of the hydrogel beads solely relying on hydrogen bonding among the protonated sulfate groups of fucoidan, the carboxyl groups of carboxymethyl chitosan hydrogel, and the hydroxyl groups of curcumin under acidic condition, thereby eliminating the need for chemical modifiers. The strategy exploits the intrinsic functional groups of readily available food biopolymers and bioactive compounds to enable a practical and green strategy for the encapsulation of other natural phenolic compounds.



1                    **Preparation and Characterization of pH-Responsive**  
2                    **Fucoidan/Carboxymethyl Chitosan Hydrogel Beads for Curcumin**  
3                    **Encapsulation and in vitro Gastrointestinal Release**  
4  
5

6                    Jiayu Yu<sup>a</sup>, Hongyang Hu<sup>a</sup>, Yingyi Wang<sup>a</sup>, Xia Sun<sup>a</sup>, Hanxu Li<sup>a</sup>, Shun Xiao<sup>a</sup>, Bingcan  
7                    Chen<sup>b,\*</sup>, Hui Li<sup>a,\*</sup>

8  
9                    <sup>a</sup>*College of Food Science and Engineering, Jilin University, Changchun, Jilin, 130062,*  
10                    *China*

11                    <sup>b</sup>*Department of Plant Sciences, North Dakota State University, Fargo, ND 58108,*  
12                    *United States*

13                    \* Corresponding authors: Bingcan Chen, Hui Li

14                    E-mail: bingcan.chen@ndsu.edu (B. Chen), lihuiqq23@jlu.edu.cn (H. Li)

15



16 **Abstract**

17 Curcumin (Cur) features versatile bioactivities but suffers from poor stability and  
18 high vulnerability to gastrointestinal degradation. To address these bottlenecks, an  
19 effective and facile strategy for constructing a sustainable hydrogel delivery system  
20 with pH-responsive function and controlled gastrointestinal release properties is  
21 reported. The hydrogel beads were developed through physical crosslinking between  
22 fucoidan (Fuc), carboxymethyl chitosan (CMCS), and the encapsulated bioactive  
23 compound Cur. Structural characterization confirmed that intermolecular hydrogen  
24 bonding between Fuc and CMCS played a pivotal role in the hydrogel network  
25 formation. Cur was efficiently encapsulated within the hydrogel beads, functioning as  
26 an additional crosslinking agent that increased the crosslinking density and reduced the  
27 equilibrium water content of the system. Notably, the hydrogel beads protected Cur via  
28 non-covalent interactions and physical barriers, enhancing its thermal and UV  
29 stabilities. Furthermore, the hydrogel beads exhibited pronounced pH-responsive  
30 swelling and release behaviors, showing minimal swelling and limited release in acidic  
31 gastric conditions, in contrast to sharp swelling and near-complete release in alkaline  
32 intestinal environments, attributed to the pH-dependent protonation states of  
33 polysaccharides' functional groups altering intermolecular interactions. Importantly,  
34 the encapsulated Cur retained more than 90% antioxidant capacity following simulated  
35 gastrointestinal digestion. This crosslinker-free and food-grade system provides a safe  
36 delivery platform for labile polyphenols, showing considerable potential in functional  
37 foods and dietary supplements.



38 **Keywords:** fucoidan; carboxymethyl chitosan; pH-responsive hydrogel beads,

[View Article Online](#)

[DOI: 10.1039/D6FB00033A](https://doi.org/10.1039/D6FB00033A)

39 curcumin; oral delivery system; controlled release



## 40 1. Introduction

41 With the rising consumer demand for functional foods that integrate nutrition and  
42 health benefits, the food industry has increasingly focused on incorporating food-  
43 derived bioactive compounds (e.g., polyphenols, vitamins, and bioactive lipids) into  
44 daily products. Curcumin (Cur), a natural polyphenol derived from *Curcuma longa* L.,  
45 has attracted extensive attention in food science and nutrition owing to its versatile  
46 bioactivities, including antioxidant, anti-inflammatory, gut-protective, and chronic  
47 disease-mitigating properties.<sup>1</sup> However, the direct utilization of Cur in food systems is  
48 severely hindered by inherent physicochemical limitations, such as extremely low  
49 water solubility, poor chemical stability, and rapid degradation in the gastrointestinal  
50 tract (GIT),<sup>2</sup> which collectively result in low bioavailability and compromised  
51 functional efficacy. Hence, addressing these challenges is critical for unlocking the full  
52 application potential of Cur in formulating it into the existing food products.

53 To overcome the delivery bottlenecks of Cur, various encapsulation systems have  
54 been developed over the past decades, such as lipid-based carriers, protein-based  
55 matrices, polymeric nanoparticles, and microcapsules.<sup>3, 4</sup> Despite the fact that these  
56 systems have shown certain effects in improving the stability and bioavailability of Cur,  
57 they share inherent limitations, such as the susceptibility to lipid oxidation, high  
58 sensitivity to pH, temperature, and enzymatic degradation.<sup>5</sup> Hence, there remains an  
59 urgent need to develop a biocompatible, stable, and cost-effective delivery system that  
60 can efficiently protect Cur during food processing and after ingestion.

61 Food biopolymer based hydrogels are three-dimensional network materials



62 formed by polysaccharides and/or proteins in aqueous microenvironments, whose  
63 tunable physicochemical properties enable responsiveness to environmental stimuli.<sup>6</sup>  
64 Specifically, their pH-sensitivity has attracted significant attention for oral food  
65 applications, as they can adapt to the distinct pH gradients of the GIT.<sup>7</sup> Such systems  
66 protect bioactive compounds in acidic gastric environments while triggering release in  
67 the intestine via pH-responsive mechanisms. Fucoidan (Fuc), a sulfated polysaccharide  
68 rich in sulfate groups from brown algae, exhibits diverse bioactivities, including  
69 antioxidant activity, anti-tumor, immunomodulatory, and antithrombotic.<sup>8,9</sup> The sulfate  
70 groups in Fuc chain undergo pH-dependent protonation/deprotonation (pKa 1.0-2.5)  
71 and endow correspondingly gastric pH responsiveness.<sup>10</sup> Carboxymethyl chitosan  
72 (CMCS) is a versatile chitosan derivative containing adequate amino and carboxyl  
73 groups and combines chitosan's biocompatibility with superior water solubility and  
74 pKa values of 6.5 and 2.7 within the gastrointestinal pH range.<sup>11, 12</sup> Importantly,  
75 CMCS's anionic nature enables miscibility with Fuc in aqueous solutions which avoids  
76 the development of insoluble polyelectrolyte complexes.<sup>11</sup> Despite the favorable  
77 properties of Fuc and CMCS, Fuc alone lacks sufficient gelling ability, limiting its  
78 direct application in hydrogel fabrication.<sup>13</sup> Therefore, certain chemical crosslinking  
79 strategies such as aldehyde modification of Fuc or EDC/NHS coupling have been  
80 reported to prepare Fuc-CMCS hydrogels.<sup>14, 15</sup> However, these chemical approaches  
81 involve toxic reagents, complicated modification procedures, and potential food safety  
82 risks, which violate the principles of green and sustainable food processing.  
83 Additionally, such conventional methods overlook the presence of abundant hydroxyl



84 and sulfate groups in Fuc as well as the carboxyl, amino, and hydroxyl groups in CMCS,  
85 which may potentially provide abundant sites for intermolecular hydrogen bond  
86 interactions and facilitate the assembly of stable composite hydrogels without the need  
87 for chemical modifications.

88 Building on the complementary structural features and hydrogen bond-forming  
89 capacities of Fuc and CMCS, we hypothesize that simple, green, hydrogen  
90 bond-mediated Fuc/CMCS composite hydrogel beads can effectively resolve the  
91 delivery bottlenecks of Cur. Inspired by the strong binding affinity between  
92 polyphenols and dietary polysaccharides via non-covalent interactions in natural plant  
93 cell walls,<sup>16</sup> this composite hydrogel system is expected to efficiently encapsulate and  
94 stabilize Cur via hydrogen bonds formed between the phenolic hydroxyl groups of Cur  
95 and the functional groups of Fuc and CMCS. Furthermore, the hydrogen bond-  
96 crosslinked Fuc/CMCS network will exhibit inherent pH responsiveness, as changes in  
97 GIT pH alter the stability of intermolecular interactions, thereby protecting Cur in the  
98 stomach and triggering its controlled release in the intestine.

99 Hence, this study designed and fabricated hydrogen bond-mediated physically  
100 crosslinked Fuc-CMCS hydrogel beads for Cur encapsulation. The physicochemical  
101 structure, swelling behaviors, pH responsiveness and mechanism, the stability of Cur  
102 under various conditions, and the corresponding release profiles of Cur from the  
103 hydrogel beads were thoroughly explored. Meanwhile, the free radical scavenging  
104 ability, monitored by real-time electron paramagnetic resonance (EPR) spectroscopy,  
105 was evaluated after *in vitro* simulated gastrointestinal digestion to assess both the



106 antioxidant capacity of encapsulated Cur and the protective mechanism of the hydrogel  
107 beads. This green, chemically unmodified design developed in this study follows  
108 sustainable food processing guidelines and provides a safe platform for stabilizing and  
109 delivering labile bioactive compounds, with considerable potential in functional foods  
110 and dietary supplements.

111

## 112 **2. Materials and methods**

### 113 **2.1 Materials**

114 Fuc (from: brown seaweed, purity: 98%, sulphation degree: 0.24, molecular  
115 weight: 121.6 kDa) was purchased from Macklin Biochemical Technology Co., Ltd.  
116 (Shanghai, China). CMCS (carboxylation degree:  $\geq 80\%$ , deacetylation degree: 88%-  
117 92%, molecular weight: 100 kDa), Cur, polyethylene glycol 400 (PEG400), and 1,1-  
118 diphenyl-2-picrylhydrazyl (DPPH) were supported by Aladdin Biochemical  
119 Technology Co., Ltd. (Shanghai, China). Trypsin (from porcine pancreas), pepsin (pig  
120 source), and bile salt (pig source) were supplied by Macklin Biochemical Technology  
121 Co., Ltd. (Shanghai, China).

### 122 **2.2 Preparation of Fuc-CMCS@Cur hydrogel beads**

123 Specifically, Fuc and CMCS were separately dissolved in deionized water to  
124 prepare polysaccharide solutions with a concentration of 5% (w/v). A 0.5 mg mL<sup>-1</sup> Cur  
125 solution was prepared by dissolving in a PEG400/deionized water mixture with a  
126 volume ratio of 1:3. PEG400, a FDA approved food-grade polymer, served to enhance  
127 the dispersibility of Cur in deionized water, thereby facilitating the uniform dispersion



128 of Cur within the hydrogel matrix.<sup>17</sup> To prepare Cur-encapsulated hydrogel beads, the  
129 Cur stock solution was thoroughly blended with equal volumes of Fuc and CMCS  
130 solutions under gentle stirring to ensure homogeneous mixing. The obtained mixed  
131 solution was then slowly and carefully added dropwise into 0.1 M HCl solution using  
132 a 10  $\mu$ L pipette tip to induce gelation and beads formation. The reaction was allowed  
133 to proceed for 1 h to ensure complete crosslinking, even though the hydrogel beads  
134 formed instantaneously. Finally, the as-prepared hydrogel beads (denoted  
135 Fuc-CMCS@Cur) were collected and washed three times with deionized water to  
136 remove residual surface components, and then used for subsequent characterization and  
137 analysis. A control of mixed Fuc and CMCS was prepared following the same  
138 procedure but replacing the Cur with the same volume of deionized water.

### 139 2.3 Encapsulation efficiency (*EE*) and loading capacity (*LC*)

140 To evaluate the *EE* and *LC* of the hydrogel beads system, the prepared hydrogel  
141 beads were transferred to ethanol to extract Cur with the assistance of ultrasound.  
142 Subsequently, the insoluble polysaccharides were precipitated by centrifugation (12  
143 000 rpm, 2 min), and the supernatant was carefully collected. The concentration of Cur  
144 in the supernatant was measured by recording the absorbance at 426 nm using a UV-  
145 vis spectrophotometer. The amount of encapsulated Cur was determined by referring  
146 to a standard curve. The Cur-encapsulated hydrogel beads were then freeze-dried for  
147 *LC* determination. The *EE* and *LC* were calculated using the following equations:

$$148 \quad EE (\%) = \text{mass of encapsulated Cur} / \text{mass of added Cur} \times 100\%$$

$$149 \quad LC (\%) = \text{mass of encapsulated Cur} / (\text{mass of beads} + \text{mass of encapsulated Cur}) \times 100\%$$



## 150 **2.4 Structural characterization**

151 Fourier transform infrared (FTIR) spectra of the samples were recorded ranging  
152 from 4000-400  $\text{cm}^{-1}$  by a FTIR spectrometer (BRUKER Vertex 70) equipped with an  
153 attenuated total reflectance (ATR) module. The spectra were obtained by accumulating  
154 32 scans at a resolution of 4  $\text{cm}^{-1}$ . X-ray diffraction (XRD) data were conducted by an  
155 X-ray powder diffractometer (BRUKER D8 ADVANCE) with a voltage of 40 kV and  
156 a current of 40 mA, utilizing Cu  $K\alpha$  radiation ( $\lambda = 1.5406 \text{ \AA}$ ). The samples were scanned  
157 over a diffraction angle  $2\theta$  range from 5 to 50° at a scanning rate of 5°  $\text{min}^{-1}$ .  
158 Thermogravimetric analysis (TGA) was performed using a TA Instruments Q50  
159 thermogravimetric analyzer under a nitrogen atmosphere with a flow rate of 30  $\text{mL min}^{-1}$ .  
160 The samples were placed in an alumina crucible and heated from 30 to 600 °C at a  
161 heating rate of 10 °C  $\text{min}^{-1}$ . Scanning electron microscope (SEM, Zeiss-Merlin Gemini  
162 SEM 300) was used to observe the surface and cross-sectional morphologies of freeze-  
163 dried samples at an acceleration voltage of 5 kV. The UV-vis absorption spectroscopy  
164 was measured ranging from 250-550 nm by using a Perkin Elmer Lambda 35 UV-vis  
165 spectrophotometer. The samples were placed in a 10 mm path length quartz cuvette for  
166 the measurement.

## 167 **2.5 Thermal and UV stabilities**

168 Free Cur solution and Fuc-CMCS@Cur hydrogel beads with equal weight of Cur  
169 were subjected to different treatments. They were placed in the dark at 4, 20, 37, 60,  
170 and 80 °C for 1 h, or in the dark at 80 °C for 3 h, or under 365 nm UV irradiation for 3  
171 h. Subsequently, the absorbance of the solutions was measured at 426 nm using a UV-



172 vis spectrophotometer to assess the retention of Cur in the samples. The Cur retention  
173 rate was calculated using the following formula:

174 Cur retention rate (%) = mass of Cur in treated samples under different conditions / mass of Cur  
175 in untreated samples  $\times$  100%

## 176 2.6 Measurement of the pH-sensitive swelling behavior

177 Equilibrium water content (EWC) of hydrogel beads was determined as  
178 follows.<sup>18</sup> The samples were soaked in deionized water at room temperature to achieve  
179 their equilibrium swelling. The weight of swollen hydrogel beads was denoted as  $W_s$   
180 Subsequently, these swollen hydrogel beads were freeze-dried and weighed as  $W_d$  The  
181 EWC was calculated according to the following equation:

$$182 \text{ EWC (\%)} = (W_s - W_d) / W_d \times 100\%$$

183 The swelling behavior of the hydrogel beads was investigated by a weighing  
184 method. Briefly, the freeze-dried samples were accurately weighed and designated as  
185  $M_1$ . These samples were then placed in separate petri dishes, each containing an equal  
186 volume of medium solutions with varying pH values (2.0, 4.0, 6.0, and 7.4). After 4 h,  
187 the swollen samples were carefully taken out from the solutions. Excess liquid on the  
188 surface of the samples was gently blotted off using filter paper, and the samples were  
189 subsequently weighed as  $M_2$ . The swelling degree was calculated using the following  
190 formula:

$$191 \text{ Swelling degree (\%)} = (M_2 - M_1) / M_1 \times 100\%$$

192 The size of swollen hydrogel beads was determined by particle sizing analysis  
193 software, and the mean size change rate was calculated using the following equation:



194 Mean size change rate (%) =  $(D_s - D_{fd}) / D_{fd} \times 100\%$

195 where  $D_s$  represents the mean size of swollen hydrogel beads and  $D_{fd}$  represents the  
196 mean size of freeze-dried hydrogel beads.

## 197 **2.7 Measurement of the pH-sensitive release behavior**

198 The pH-sensitivity of the hydrogel beads was evaluated by studying the release  
199 profile of Cur from the hydrogel beads in medium solutions with different pH values  
200 (2.0, 4.0, 6.0, and 7.4). Specifically, the Fuc-CMCS@Cur hydrogel beads were  
201 separately incubated in various pH-adjusted medium solutions for 4 h. At 30-minute  
202 intervals, 0.1 mL of the supernatant was withdrawn for Cur determination and  
203 immediately replaced with fresh medium to maintain constant volume. The withdrawn  
204 supernatant was then mixed with 0.9 mL of ethanol. The absorbance of Cur in the  
205 supernatant was measured at 426 nm using a UV-vis spectrophotometer.

## 206 **2.8 *In vitro* simulated gastrointestinal environment release**

207 The simulated gastric fluids (SGF, pH 2.0) and simulated intestinal fluids (SIF,  
208 pH 7.0) were prepared according to the methods with some modification.<sup>19</sup> Briefly,  
209 SGF was prepared by adjusting a 0.2% (w/v) NaCl solution to pH 2.0 with a 1.0 M HCl  
210 solution. A specific amount of gastric protease was added to the solution to achieve a  
211 final concentration of 3.0% (w/v). For the SIF, trypsin and bile salt were evenly  
212 dispersed in a PBS buffer (pH 7.0) with final concentrations of 1.0% and 0.8% (w/v),  
213 respectively. Subsequently, the pH value of the mixture was adjusted to 7.0 using a 1.0  
214 M NaOH solution.

215 To investigate the release profile of Cur from the hydrogel beads, the Fuc-



216 CMCS@Cur hydrogel beads were initially incubated in the SGF at 37 °C for 2 h. After  
 217 that, the hydrogel beads were transferred to the SIF and maintained at 37 °C for 4 h. At  
 218 30-minute intervals, 0.1 mL of the supernatant was withdrawn for the determination of  
 219 Cur and replaced with fresh medium to keep the volume constant. The withdrawn  
 220 supernatant was mixed with 0.9 mL of ethanol, and the absorbance of Cur in the  
 221 supernatant was measured at 426 nm using a UV-vis spectrophotometer.

## 222 2.9 DPPH radical scavenging capacity test

223 The DPPH radical scavenging capacity of samples was determined by electron  
 224 paramagnetic resonance (EPR) spectroscopy. In detail, the hydrogel beads that had been  
 225 digested by either SGF (2 h) or SIF (4 h) were mixed with 0.2 mM DPPH ethanol  
 226 solution by the equal volume. Immediately after mixing, the EPR signal of DPPH was  
 227 monitored. The hydrogel beads incubated in PBS (pH 7.4) served as the control group.  
 228 The double-integration of the EPR spectrum, commonly known as the EPR signal, was  
 229 then used to determine the extent of DPPH reduction according to the following  
 230 formula:<sup>20</sup>

$$231 \quad \text{EPR signal reduction (\%)} = (S_{\text{DPPH}} - S_{\text{sample}}) / S_{\text{DPPH}} \times 100\%$$

232 where  $S_{\text{DPPH}}$  represents the EPR signals for free DPPH ethanol solution and  $S_{\text{sample}}$   
 233 represents the EPR signals of hydrogel beads.

234 The antioxidant kinetic process of hydrogel beads was determined by single  
 235 exponential or biexponential fitting kinetic parameters using the following formula:<sup>20</sup>

$$236 \quad \text{EPR}_{\text{signal}} = S_0 + A \exp(-(t-t_0) / t_1)$$

$$237 \quad \text{EPR}_{\text{signal}} = S_0 + A \exp(-(t-t_0) / t_1) + B \exp(-(t-t_0) / t_2)$$



238 where EPR signal denotes the double integration of the DPPH scavenging EPR  
239 spectrum along time, while  $t_1$  and  $t_2$  correspond to the time constants for the DPPH  
240 decay of two different antioxidant processes, respectively.

## 241 **2.10 Statistical analysis**

242 All experiments were performed in triplicate and results were analyzed using  
243 IBM SPSS software. One-way ANOVA with Tukey test was applied for significance  
244 tests, and differences were considered significant if  $p < 0.05$ .

## 245 **3. Results and discussion**

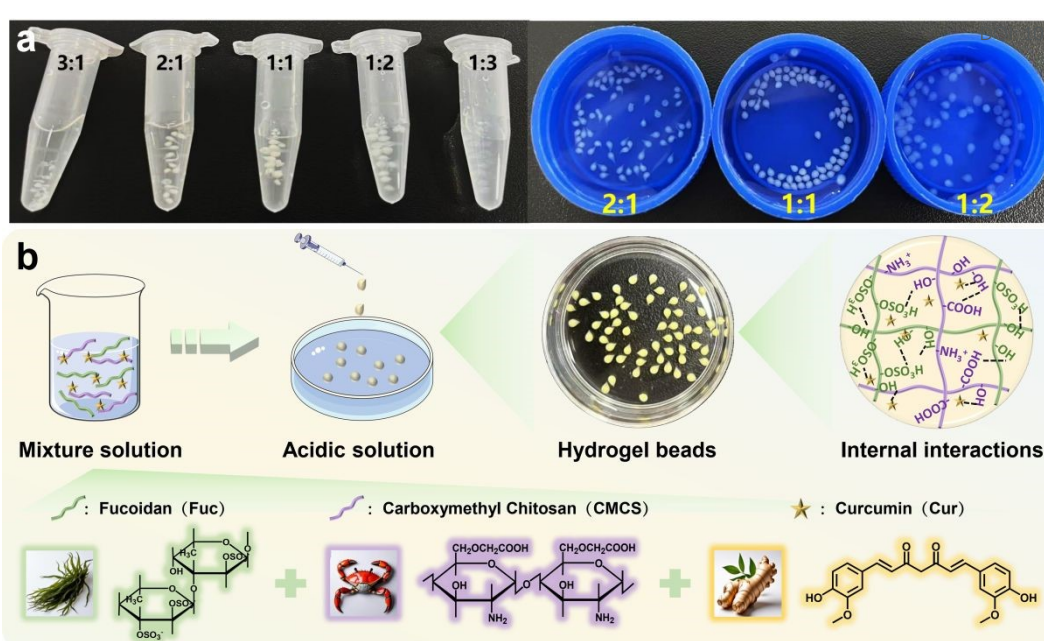
### 246 **3.1 Preparation of Fuc-CMCS and Fuc-CMCS@Cur hydrogel beads**

247 As expected, individual biopolymer solutions (pure Fuc or CMCS) could not  
248 form hydrogel beads under our experimental condition. Interestingly, we observed that  
249 hydrogel beads were able to form by the mixture of Fuc and CMCS solutions under the  
250 acidic environment. In order to better compare the role of Cur on the properties of the  
251 hydrogel beads formed by Fuc and CMCS, we first optimized the volume ratio of the  
252 Fuc and CMCS mixture. To do so, the mixed solution of Fuc and CMCS with various  
253 volume ratios (3:1, 2:1, 1:1, 1:2, 1:3) was injected dropwise into a 0.1 M HCl solution  
254 to prepare hydrogel beads. As shown in Fig. 1a, the fabricated hydrogel beads displayed  
255 characteristic spherical morphology with uniform white color and were dependent on  
256 Fuc/CMCS volume ratios. Specifically, a concentration-dependent morphological  
257 alteration was observed with the increase of Fuc content, manifested by progressive  
258 opacity enhancement, measurable size reduction, and pronounced tailing formation,  
259 suggesting the gradual densification of the three-dimensional polymeric network



260 structure. Meanwhile, extreme mixing volume ratios (Fuc/CMCS  $\geq$  3:1 or  $\leq$  1:3) could  
261 not produce stable spherical architectures. This phenomenon stemmed from  
262 competitive hydrogen bonding interactions in Fuc/CMCS/water system where  
263 individual polysaccharide (Fuc or CMCS) preferentially engaged in hydration with  
264 water molecules rather than forming inter-polymer crosslinks, resulting in failure to  
265 form a three-dimensional network structure. Accordingly, a Fuc/CMCS volume ratio  
266 of 1:1 was selected to prepare the optimized control sample (Fuc-CMCS) as well as the  
267 Cur-encapsulated hydrogel beads (Fuc-CMCS@Cur) following the identical procedure  
268 as described in section 2.2 and illustrated in Fig. 1b. Regarding the appearance of Fuc-  
269 CMCS@Cur, no other notable alterations were observed except the unmistakable  
270 yellow color of the hydrogel beads (Fig. 1b). The encapsulation efficiency (*EE*) and  
271 loading capacity (*LC*) of the hydrogel beads for Cur were determined to be 88.22% and  
272 3.45 mg g<sup>-1</sup>, respectively. The high *EE* value could be ascribed to the strong  
273 intermolecular hydrogen bonding interactions between Cur and the Fuc-CMCS  
274 polysaccharide network, which effectively trapped Cur molecules inside the hydrogel  
275 matrix during the acidic gelation process. Meanwhile, the considerable *LC* value  
276 indicated that the hydrogel beads exhibited favorable loading potential for hydrophobic  
277 Cur, wherein food-grade PEG400 promoted Cur uniform dispersion and facilitated its  
278 homogeneous integration into the hydrogel network.



View Article Online  
039/D6FB00033A

279

280 **Fig. 1.** (a) Digital photographs of the freshly prepared hydrogel beads with various  
 281 volume ratios of Fuc/CMCS; and (b) schematic diagram for preparation and  
 282 crosslinking mechanism of Fuc-CMCS@Cur hydrogel beads.

283

284 **3.2 Characterization of Fuc-CMCS hydrogel beads and Fuc-CMCS@Cur**  
 285 **hydrogel beads**

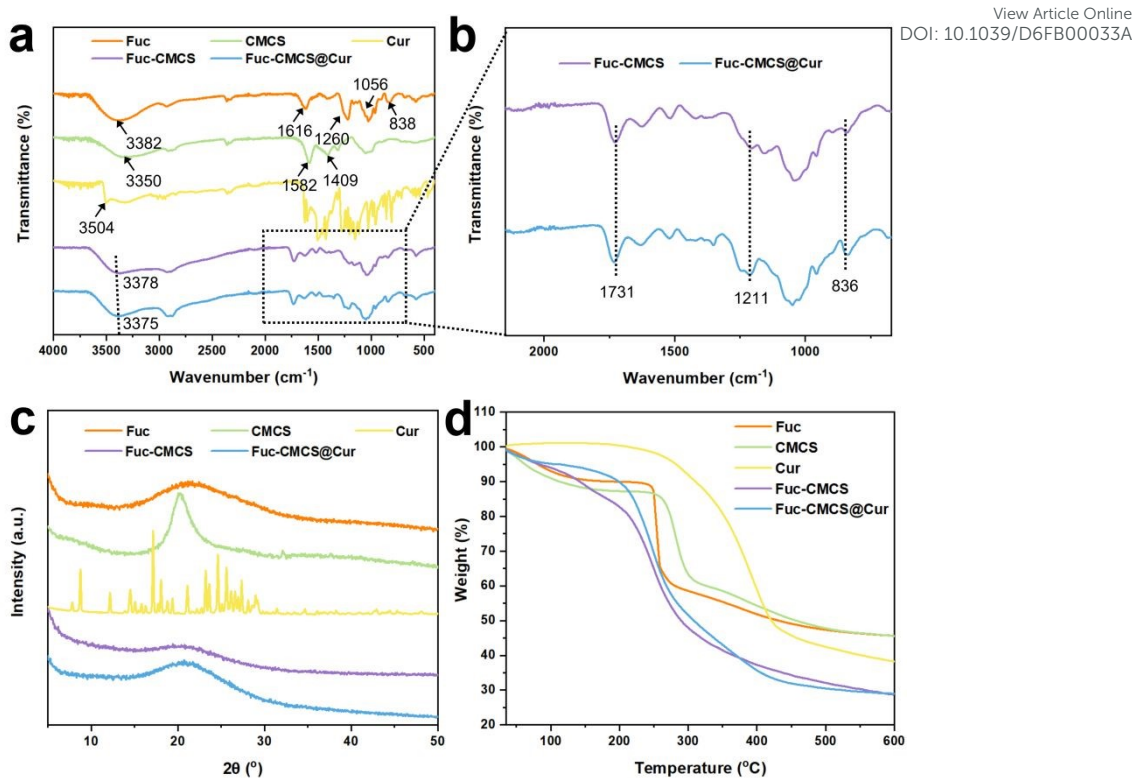
286 **3.2.1 Structural and physical properties**

287 Given that FTIR can evaluate the interactions among different components within  
 288 composite hydrogel beads, the FTIR spectra of Fuc, CMCS, Cur, Fuc-CMCS, and Fuc-  
 289 CMCS@Cur hydrogel beads were determined (Fig. 2a). The FTIR spectra of Fuc,  
 290 CMCS, and Cur exhibited broad absorption peaks in the range of 3000-3600  $\text{cm}^{-1}$ ,  
 291 corresponding to the -OH stretching vibration. Additionally, a characteristic peak  
 292 observed at approximately 2800  $\text{cm}^{-1}$  was assigned to C-H stretching vibrations.<sup>21</sup> For  
 293 Fuc, the absorption peak at 1616  $\text{cm}^{-1}$  was associated with the presence of 2-O-acetyl  
 294 groups in the structure. A broad band in the range of 1222-1260  $\text{cm}^{-1}$  corresponded to



295 the stretching vibration of S=O, and the absorption peak at 838 cm<sup>-1</sup> was related to the  
296 stretching vibration of C-O-S.<sup>22</sup> For CMCS, a broad absorption peak at 3000-3600 cm<sup>-1</sup>  
297 <sup>1</sup> was also assigned to stretching vibrations of N-H. The characteristic peaks at 1582  
298 and 1409 cm<sup>-1</sup> originated from the asymmetric and symmetric stretching vibrations of  
299 -COO<sup>-</sup>.<sup>23</sup> By contrast, the spectra of Fuc-CMCS and Fuc-CMCS@Cur hydrogel beads  
300 showed several significant alterations. A new peak appeared at 1211 cm<sup>-1</sup> potentially  
301 attributed to the protonation of -NH<sub>2</sub> groups within the CMCS chain.<sup>24</sup> Moreover, the  
302 newly observed characteristic peak at 1731 cm<sup>-1</sup> (Fig. 2b) corresponded to the  
303 protonated carboxyl groups (-COOH) in CMCS.<sup>25</sup> These protonated functional groups  
304 could readily form intermolecular hydrogen bonding interactions with the -OH groups  
305 present in both Fuc and Cur. The characteristic absorption peak at 838 cm<sup>-1</sup>, assigned  
306 to the C-O-S stretching vibration of sulfate groups in Fuc, exhibited a noticeable shift  
307 to 836 cm<sup>-1</sup> after hydrogel bead formation (Fig. 2b).<sup>26, 27</sup> According to previous reports,  
308 this shift was typically induced by hydrogen bond formation between sulfate groups in  
309 Fuc and hydroxyl groups in CMCS and Cur.<sup>10</sup> Furthermore, the broad absorption band  
310 associated with -OH stretching was shifted from 3378 cm<sup>-1</sup> in Fuc-CMCS to 3375 cm<sup>-1</sup>  
311 <sup>1</sup> in Fuc-CMCS@Cur. This change further confirmed the formation of hydrogen  
312 bonding interactions between Cur and the Fuc-CMCS polysaccharide network,<sup>28</sup>  
313 collectively demonstrating that Cur was successfully encapsulated within the hydrogel  
314 beads. The significant overlap between the main absorption bands of Cur and those of  
315 polysaccharides, coupled with the low content of Cur, likely accounted for the minimal  
316 alterations observed in the FTIR after Cur encapsulation.<sup>29</sup>



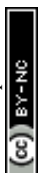


317

318 **Fig. 2.** (a) Raw and (b) enlarged FTIR spectra, (c) XRD patterns, and (d) TGA  
 319 thermograms of Fuc, CMCS, Cur, Fuc-CMCS hydrogel beads and Fuc-CMCS@Cur  
 320 hydrogel beads.

321

322 XRD was employed to investigate the crystal or amorphous structural changes of  
 323 the hydrogel beads matrix and Cur (Fig. 2c). The characteristic broad diffraction peaks  
 324 of Fuc and CMCS were found at  $2\theta = 22.8^\circ$  and  $20.2^\circ$ , respectively, indicating their  
 325 amorphous state. The XRD diffraction patterns of Fuc-CMCS and Fuc-CMCS@Cur  
 326 hydrogel beads exhibited even broader and weaker peaks in the same angular region.  
 327 This transformation primarily resulted from competitive hydrogen bonding interactions  
 328 between Fuc and CMCS, specifically disrupting the formation of individual hydrogen  
 329 bonds and altering the crystalline region of polysaccharides.<sup>30</sup> Notably, free Cur  
 330 manifested a distinguishable crystalline structure. However, for Fuc-CMCS@Cur  
 331 hydrogel beads, the characteristic diffraction peaks of free Cur disappeared entirely,



332 which was probably attributed to the intermolecular interactions that took place  
333 between Cur and polysaccharide matrix during the encapsulation procedure. Such  
334 interactions led to the obscuration or alteration of the molecular arrangement of Cur  
335 upon encapsulation. Consequently, there was a transition of Cur from a crystalline state  
336 to an amorphous state.<sup>31</sup>

337 The thermal properties of Cur, polysaccharides, and the formed hydrogel beads  
338 were assessed using TGA (Fig. 2d). In the case of pure Fuc and CMCS, the first stage  
339 degradation occurred within a temperature range of approximately 30-220 °C, which  
340 was mainly caused by the diffusion loss of free water and bound water within Fuc and  
341 CMCS, accompanied by the partial cleavage of glycosidic bonds.<sup>32</sup> The second stage  
342 corresponded to a temperature range of 220-340 °C, and was predominantly  
343 characterized by the cleavage of glycosidic bonds presented within the structural units  
344 of Fuc and CMCS. Moreover, during this particular stage, adjacent hydroxyl groups  
345 were eliminated in the form of water molecules, and eventually, the intermediate  
346 products experienced carbonization and decomposition. Conversely, the thermal  
347 decomposition patterns of the hydrogel beads exhibited markedly distinct  
348 characteristics compared to the individual components. The initial degradation of the  
349 hydrogel beads was primarily caused by the loss of free water and bound water within  
350 the temperature range of 30-190 °C. At 190 °C, Fuc-CMCS exhibited 15.87% weight  
351 loss when compared to 8.90% for Fuc-CMCS@Cur, indicating that the latter contained  
352 less water. This phenomenon was likely due to the addition of Cur, which weakened  
353 the interaction between the polysaccharide matrix and water, thereby reducing available



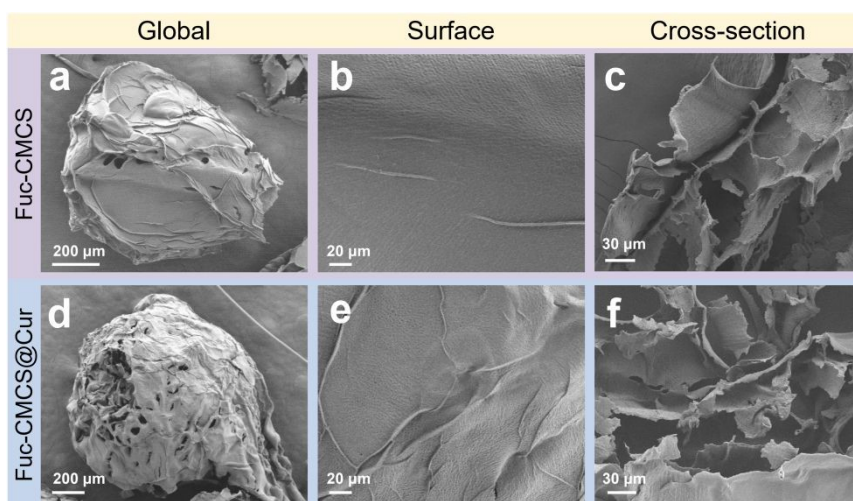
354 sites for water coordination. Subsequently, the notable weight loss in the temperature  
355 range of 190-350 °C could be ascribed to the disruption of polysaccharide  
356 intramolecular and intermolecular interactions, caused by the depolymerization of  
357 molecular rings along with the cleavage of saccharide rings and glycosidic bonds.<sup>32</sup> The  
358 weight loss of Fuc-CMCS@Cur hydrogel beads at 350-430 °C was probably due to the  
359 decomposition of Cur, as evidenced by the curve of free Cur. Finally, the hydrogel  
360 beads' matrix underwent gradual thermal decomposition at a higher temperature of 430-  
361 600 °C.<sup>33</sup>

### 362 3.2.2 Morphology and microstructure

363 The surface and cross-sectional morphologies, as well as microstructures of  
364 lyophilized Fuc-CMCS and Fuc-CMCS@Cur hydrogel beads were characterized by  
365 SEM (Fig. 3). The surface of the hydrogel beads displayed folding patterns and  
366 depressions, which could be attributed to the dehydration shrinkage of the hydrogel  
367 networks during the freeze-drying process (Fig. 3a & d).<sup>34, 35</sup> For the microstructure of  
368 Fuc-CMCS hydrogel beads, it exhibited minimal wrinkles and folds on the surface.  
369 This indicated that polysaccharide-only composition restricted the mobility of water  
370 within the hydrogel beads, thereby promoting the formation of a smaller and more  
371 compact network structure (Fig. 3a).<sup>36</sup> Upon the incorporation of Cur, the hydrogel bead  
372 structure became larger and more wrinkled (Fig. 3d), which was probably attributed to  
373 the competitive replacement of Cur with water molecules within the polysaccharide  
374 matrix, forming stable hydrogen bonds with the polymer chains. This molecular  
375 interaction diminished the water-holding capacity of hydrogel beads, making the water



376 molecules more susceptible to being squeezed out by external forces, thereby yielding  
 377 a characteristically coarser microstructure. Furthermore, magnification images revealed  
 378 that all the hydrogel beads exhibited dense surface structures without any clearly visible  
 379 micropores and particles (Fig. 3b & e). This suggested that the Cur molecules dispersed  
 380 well in the hydrogel matrix which could provide superior protective effects.<sup>35</sup> The  
 381 cross-sectional images showed that both Fuc-CMCS and Fuc-CMCS@Cur hydrogel  
 382 beads featured a characteristic honeycomb-like network structure (Fig. 3c & f).  
 383 Nevertheless, a more densely packed pore arrangement within the hydrogel network  
 384 was observed with the incorporation of Cur. This disparity could be ascribed to the  
 385 robust hydrogen bonding interactions established between Cur and Fuc-CMCS matrix.  
 386 These enhanced interactions promoted the development of a more tightly knit and  
 387 compact hydrogel network.<sup>37</sup>



388  
 389 **Fig. 3.** SEM images of the surface and cross-section of the Fuc-CMCS hydrogel beads  
 390 and Fuc-CMCS@Cur hydrogel beads.

### 391 **3.3 The thermal and UV stabilities of Cur encapsulated in Fuc-CMCS@Cur** 392 **hydrogel beads**

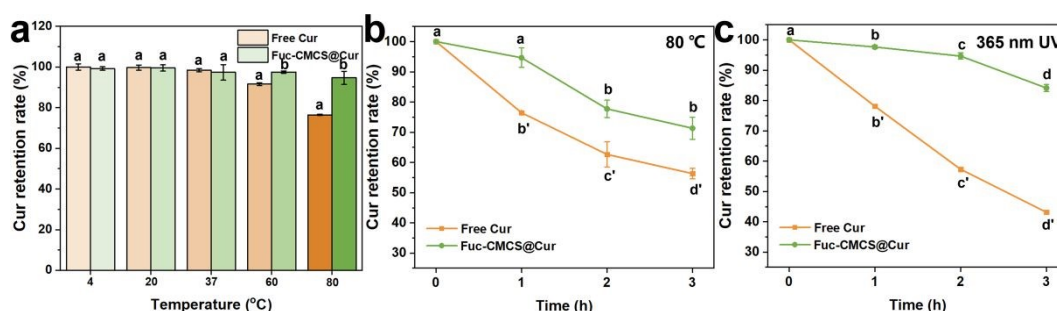
393 Considering the well-documented thermal and photochemical instability of Cur,



394 the stability of Cur within the composite hydrogel beads when exposed to thermal  
395 conditions (4, 20, 37, 60, and 80 °C) and UV irradiation ( $\lambda = 365$  nm) was examined  
396 by closely observing the degradation behaviors of both free and encapsulated Cur.  
397 According to Fig. 4a, both free and encapsulated Cur exhibited comparable retention  
398 rates without notable influence under mild temperature conditions (4, 20, and 37 °C).  
399 In contrast, upon elevating temperatures (60 and 80 °C), hydrogel beads displayed a  
400 striking protective advantage in 1 h of storage. We further prolonged the thermal  
401 treatment duration to 3 h at 80 °C to evaluate the long-term stability of Cur (Fig. 4b).  
402 Free Cur underwent rapid and severe thermal degradation under such conditions, with  
403 only approximately 50% of the initial content retained after 3 h of incubation. In sharp  
404 comparison, Cur encapsulated within the Fuc-CMCS@Cur hydrogel beads remained at  
405 a significantly higher retention level throughout the high-temperature storage. These  
406 results clearly validated that the hydrogel beads matrix exerted outstanding protective  
407 effects against thermal decomposition of Cur. The improved thermal stability was  
408 mainly attributed to the robust physical barrier provided by the polysaccharide network,  
409 which effectively isolated Cur from heat-induced degradation. Regarding UV stability  
410 (Fig. 4c), free Cur retained only 43.14% of its initial content after 3 h of continuous  
411 exposure to 365 nm UV light, indicating severe photodegradation. In contrast, Cur  
412 encapsulated in Fuc-CMCS@Cur hydrogel beads exhibited a markedly higher retention  
413 rate of up to 84.11%, demonstrating the excellent UV-shielding performance of the  
414 hydrogel system. Collectively, these findings confirmed that encapsulation within the  
415 Fuc-CMCS hydrogel beads could significantly enhance both the thermal stability and



416 UV resistance of Cur, thereby overcoming its inherent instability against harsh  
417 environmental stresses.



418

419 **Fig. 4.** Cur retention rate of Fuc-CMCS hydrogel beads and Fuc-CMCS@Cur hydrogel  
420 beads (a) at different temperatures (4, 20, 37, 60, 80 °C) for 1 h in the dark, (b) at 80 °C  
421 for 3 h in the dark, and (c) under 365 nm UV irradiation for 3 h (different letters in the  
422 figure represent significant differences at  $p < 0.05$ ).

423

### 424 3.4 The pH-sensitivity swelling and release behavior of Fuc-CMCS and Fuc- 425 CMCS@Cur hydrogel beads

426

The equilibrium water content (EWC) and swelling behavior of hydrogels are of  
427 great significance in determining the quality of their applications. These properties  
428 depend on the interactions and microstructures of the hydrogel networks, which can be  
429 used to indicate their physical or chemical crosslinking degrees in suitable solvents.<sup>18,</sup>

430

<sup>38</sup> As shown in Fig. 5a, Fuc-CMCS hydrogel beads exhibited a higher EWC compared  
431 with those encapsulated with Cur, which could be attributed to the ability of Cur to  
432 interact with the polysaccharide matrix via hydrogen bonds. Acting as a physical  
433 crosslinking agent, Cur enhanced the crosslinking degree, thereby decreasing the EWC  
434 through competitive molecular interactions. This finding was in accordance with the

435

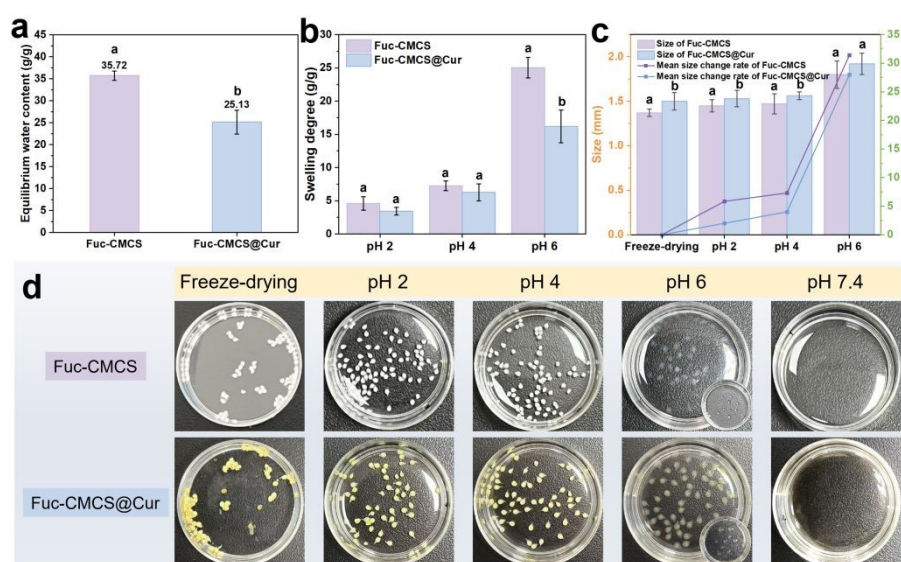
TGA and SEM results analyzed above.



436 The swelling behavior of hydrogel beads under varying pH served as a  
437 fundamental assessment of their swelling degree and size change. The freeze-dried  
438 hydrogel beads were immersed in medium solutions with different pH values (2.0, 4.0,  
439 6.0, and 7.4) for 4 h to achieve their equilibrium swelling. As shown in Fig. 5b, the  
440 swelling degrees of Fuc-CMCS hydrogel beads were higher than those of Fuc-  
441 CMCS@Cur hydrogel beads across all pH values. In the absence of Cur, a higher  
442 swelling degree and water absorption capacity was observed for Fuc-CMCS hydrogel  
443 beads. This could be attributed to its relatively loose networks and the insufficient  
444 crosslinking density, consistent with the above discussion.<sup>39</sup> Conversely, upon the  
445 addition of Cur, Cur elevated the crosslinking density of hydrogel beads by establishing  
446 hydrogen bonds with polysaccharides, which restricted the expansion space of the  
447 network structure and consequently decreased the swelling degree. This conclusion was  
448 further corroborated by the size change rates of the hydrogel beads presented in Fig. 5c  
449 & d. Specifically, across all pH values, the main size change rates of the Fuc-CMCS  
450 hydrogel beads were consistently higher than those of the Fuc-CMCS@Cur hydrogel  
451 beads. Notably, both Fuc-CMCS and Fuc-CMCS@Cur hydrogel beads demonstrated  
452 distinct swelling behaviors as the pH value changed, which revealed the pH-responsive  
453 characteristics of these hydrogel beads. The swelling degrees of these hydrogel beads  
454 at pH 2.0 and 4.0 were markedly lower compared to those at pH 6.0. Interestingly, when  
455 the pH reached 7.4, both hydrogel beads dissolved entirely, making it unfeasible to  
456 measure and compare their swelling degrees (Fig. 5d). In an environment with a  
457 relatively high concentration of H<sup>+</sup> ions (pH 2.0 and 4.0), the abundance of H<sup>+</sup> ions



458 prompted the protonation of sulfate groups in Fuc and carboxyl groups in CMCS. The  
 459 protonated groups effectively suppressed electrostatic repulsion while promoting  
 460 intermolecular hydrogen bonding, causing the matrix to become more compact with no  
 461 significant swelling. In contrast, in a weak acidic environment (pH 6.0), progressive  
 462 deprotonation of these functional groups amplified electrostatic repulsion, thereby  
 463 facilitating network expansion. Subsequently, this expansion enabled greater fluid  
 464 absorption by the hydrogel beads, manifesting as heightened swelling with larger and  
 465 more transparent shapes.<sup>32, 36</sup> While in an alkaline environment (pH 7.4), the gradual  
 466 deprotonation of amino groups in CMCS intensified electrostatic repulsion of sulfate  
 467 groups and carboxyl groups, ultimately leading to the disintegration of hydrogel beads.  
 468 The obtained results revealed that the hydrogel beads exhibited remarkable pH-  
 469 sensitivity, making them suitable for application in pH-responsive delivery systems.

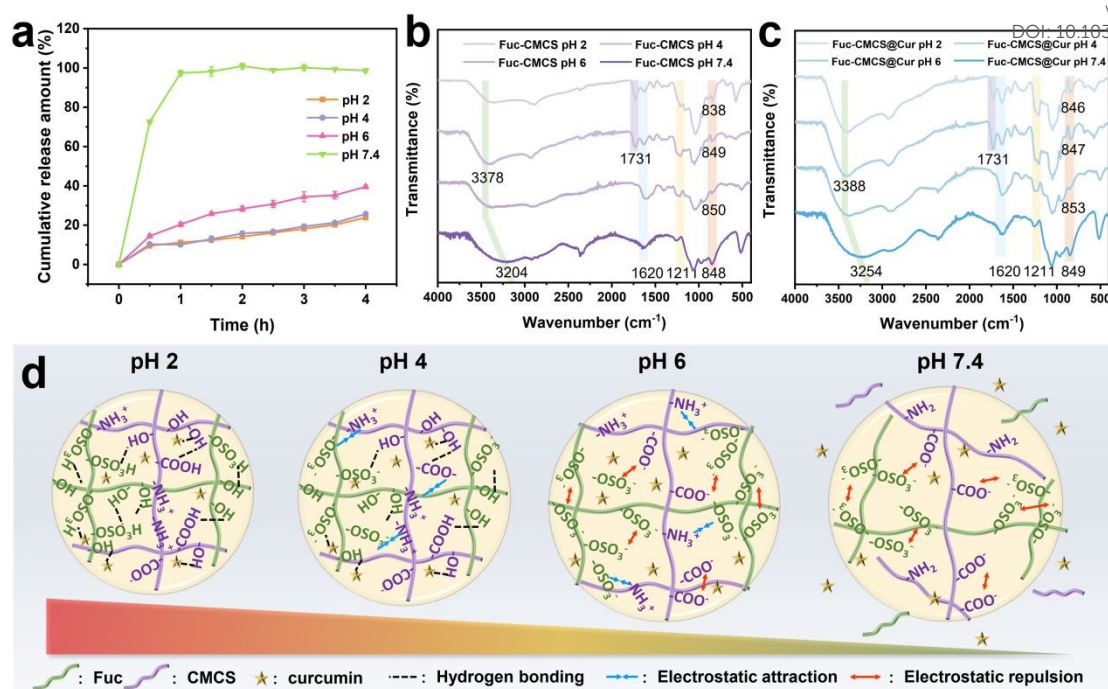


470  
 471 **Fig. 5.** (a) Equilibrium water content, (b) swelling degree, (c) size and mean size change  
 472 rate, and (d) appearance of Fuc-CMCS hydrogel beads and Fuc-CMCS@Cur hydrogel  
 473 beads under different pH conditions (different letters in the figure represent significant  
 474 differences at  $p < 0.05$ ).



475 To further demonstrate the outstanding pH-sensitivity of the hydrogel beads, the  
476 pH-dependent release profile of Cur from the hydrogel beads in medium solutions with  
477 different pH values (2.0, 4.0, 6.0, and 7.4) for 4 h was investigated and illustrated in  
478 Fig. 6a. As anticipated, Cur exhibited varying release behaviors in different pH  
479 environments. Specifically, the cumulative release amounts of Cur were only 23.84%  
480 and 22.37%, respectively, after incubating in the solution media at pH 2.0 and 4.0 for  
481 4 h. Under pH 6.0, the cumulative release amount increased to 39.56% after incubation.  
482 This increment could be explained by the significant swelling of hydrogel beads which  
483 enabled Cur to be released relatively quickly from the expandable pores of the hydrogel  
484 beads. When increasing the pH to 7.4, Cur demonstrated a rapid release behavior and  
485 reached 100% release within one hour, due to the disintegration of the hydrogel beads.  
486 The above analysis firmly confirmed that the hydrogel beads developed in this study  
487 possessed remarkable pH-sensitivity, allowing them to effectively prevent the  
488 premature release of the encapsulated Cur in an acidic environment (such as the  
489 stomach) and to facilitate a sustained release in a neutral or weakly alkaline  
490 environment (such as the intestinal tract).





491

492 **Fig. 6.** (a) Cumulative release amount of Cur from Fuc-CMCS@Cur hydrogel beads  
 493 under different pH conditions; FTIR spectra of (b) Fuc-CMCS hydrogel beads and (c)  
 494 Fuc-CMCS@Cur hydrogel beads under different pH conditions; and (d) schematic  
 495 illustrations of the interactions between Fuc and CMCS under different pH conditions.

496

497

To investigate the pH-sensitive mechanism of hydrogel beads, the FTIR spectra  
 498 of Fuc-CMCS and Fuc-CMCS@Cur hydrogel beads after the storage under various pH  
 499 conditions for 4 h were carried out and as displayed in Fig. 6b & c. The relatively low

500

content of Cur might account for the lack of significant changes in the FTIR spectra  
 501 after encapsulation.<sup>30</sup> Additionally, a schematic diagram was included in Fig. 6d to

502

provide a visual representation of the pH-sensitivity mechanism of the hydrogel  
 503 networks. At pH 2.0, the characteristic peak observed at 1731  $\text{cm}^{-1}$  was assigned to the

504

protonated carboxyl groups (-COOH) in CMCS, consistent with its pKa value of 2.7.<sup>12</sup>  
 505 Meanwhile, the peak at 838  $\text{cm}^{-1}$  corresponded to the C-O-S stretching vibration of

506

protonated sulfate groups (-OSO<sub>3</sub>H) in Fuc, whose pKa ranges from 1.0 to 2.5.<sup>10</sup> Both



507 protonated functional groups could form strong intermolecular hydrogen bonds with  
508 hydroxyl moieties present in the polysaccharide chains and Cur molecules. In addition,  
509 a distinct peak at  $1211\text{ cm}^{-1}$  appeared under acidic conditions ( $\text{pH} < 6.5$ ), which was  
510 attributed to the protonation of  $-\text{NH}_2$  to  $-\text{NH}_3^+$  in CMCS.<sup>12, 24</sup> Simultaneously, the peak  
511 at  $1620\text{ cm}^{-1}$  was ascribed to the asymmetric stretching of unprotonated carboxylate  
512 groups ( $-\text{COO}^-$ ), which only accounted for a small fraction at this low pH. At this pH,  
513 hydrogen bonding thus acted as the dominant intermolecular force that stabilized the  
514 hydrogel bead network. At pH 4.0, the spectral features showed no significant  
515 differences from those at pH 2.0, except for the shift of the peak from  $838$  to  $849\text{ cm}^{-1}$   
516 (or from  $846$  to  $847\text{ cm}^{-1}$ ). This probably indicated the deprotonation of sulfate groups  
517 ( $-\text{OSO}_3^-$ ) in Fuc due to its low pKa. As a result, it might enable electrostatic attraction  
518 with  $-\text{NH}_3^+$  in CMCS. Meanwhile, gradually deprotonated carboxyl groups could also  
519 generate such interaction with  $-\text{NH}_3^+$ . Here, the main forces acting on the hydrogel  
520 beads comprised hydrogen bonding and electrostatic attraction. At pH 6.0, the  
521 disappearance of the peak at  $1731\text{ cm}^{-1}$  and the emergence of a broad peak at  $1620\text{ cm}^{-1}$   
522 confirmed complete deprotonation of carboxyl groups. At this pH value, the dominant  
523 force within the hydrogel beads shifted to electrostatic repulsion between  $-\text{OSO}_3^-$  and  $-\text{COO}^-$ ,  
524 leading to significant swelling of hydrogel beads and correspondingly Cur  
525 release. Notably, the hydrogel beads demonstrated remarkable structural integrity  
526 without disintegration, primarily due to synergistic stabilization through hydrogen  
527 bonding and electrostatic interactions between  $-\text{NH}_3^+$  and both  $-\text{COO}^-$  and  $-\text{OSO}_3^-$   
528 groups. At pH 7.4, the peak at  $1211\text{ cm}^{-1}$  (representing  $-\text{NH}_3^+$ ) completely disappeared,



529 indicating full deprotonation of amino groups. This change intensified electrostatic  
530 repulsion between negatively charged  $\text{-COO}^-$  (from CMCS) and  $\text{-OSO}_3^-$  (from Fuc),  
531 which disrupted the original network structure and ultimately led to the disintegration  
532 of the hydrogel beads. Moreover, the broad peak underwent shifts from 3378 to 3204  
533  $\text{cm}^{-1}$  (or from 3388 to 3254  $\text{cm}^{-1}$ ) at pH 7.4, respectively. These shifts differed from  
534 those of the pure components (Fig. 2a), suggesting that the hydrogel beads' components  
535 still maintained non-covalent interactions such as hydrogen bonds.<sup>10, 34</sup>

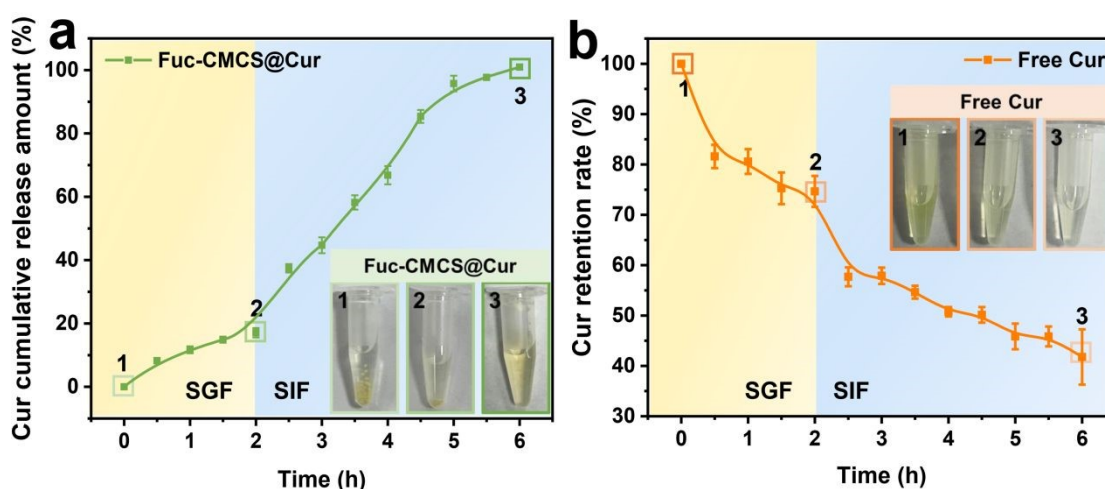
### 536 **3.5 Cur release and antioxidant activity**

#### 537 **3.5.1 The release of Fuc-CMCS@Cur hydrogel beads *in vitro* simulated** 538 **gastrointestinal environment**

539 The release profile of encapsulated Cur and retention rate of free Cur in simulated  
540 gastrointestinal fluids were checked and illustrated in Fig. 7a & b. After incubation in  
541 SGF (pH 2.0) for 2 h, the Fuc-CMCS@Cur hydrogel beads effectively retained the  
542 encapsulated Cur, and the cumulative release amount of Cur was less than 20%. This  
543 phenomenon could be ascribed to its diminished swelling capacity under acidic  
544 conditions. In contrast, the amount of Cur released from the hydrogel beads in SIF (pH  
545 7.0) increased dramatically compared to that in SGF, with approximately 100% of Cur  
546 being released within 4 h. The significantly enhanced Cur release kinetics observed in  
547 SIF could be mechanistically attributed to the pH-responsive nature and corresponding  
548 swelling behavior of the hydrogel matrix at higher pH. Notably, free Cur is highly  
549 susceptible to degradation within the human gastrointestinal tract. The controlled  
550 release behavior of Cur from the hydrogel beads effectively avoided premature



551 degradation, thereby greatly improving its bioavailability and functional efficacy. As  
 552 depicted in Fig. 7b, free Cur experienced degradation in both SGF and SIF over a 6 h  
 553 period, with only 41.77% of the initial amount remaining. These findings demonstrated  
 554 that the Fuc-CMCS@Cur hydrogel beads not only display pH-sensitive release  
 555 characteristics but also protect Cur against enzymatic degradation through a  
 556 polysaccharide matrix shield. Consequently, the encapsulated Cur achieved an almost  
 557 100% release amount, ensuring excellent active retention and delivery efficiency. These  
 558 features were also clearly demonstrated by the insets in Fig. 7a & b, which vividly  
 559 showed the release status of free and encapsulated Cur under different medium  
 560 conditions at various time points.



561  
 562 **Fig. 7.** (a) Cumulative release amount of Cur from Fuc-CMCS@Cur hydrogel beads in  
 563 simulated digestion fluids (SGF + SIF); and (b) Cur retention rate of free Cur in  
 564 simulated digestion fluids (SGF + SIF). Insets show the release or retention status of  
 565 Cur at different stages (1 represents the initial state before treatment, 2 represents the  
 566 state after completing digestion in SGF, and 3 represents the state after completing  
 567 digestion in SIF).

568

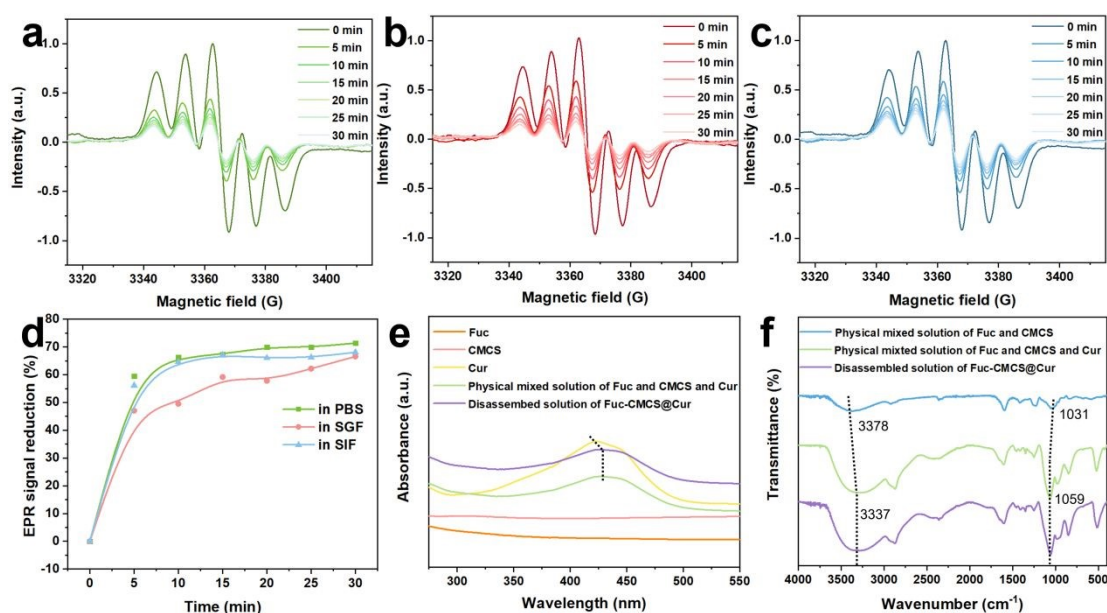
### 569 3.5.2 The antioxidant activity of Fuc-CMCS@Cur during digestion



570 Although Cur exhibits strong antioxidant properties, free Cur is highly  
571 susceptible to degradation within the human gastrointestinal environment, which  
572 significantly undermines its antioxidant activity.<sup>40</sup> Herein, EPR spectroscopy was  
573 employed to directly quantify in situ radical content in DPPH upon contact with Fuc-  
574 CMCS@Cur hydrogel beads as a function of time.<sup>41, 42</sup> A typical set of time-resolved  
575 EPR spectra of DPPH with Fuc-CMCS@Cur hydrogel beads after digestion in PBS  
576 (pH 7.4), SGF, and SIF were shown in Fig. 8a-c, respectively. At 0 min, all typical  
577 DPPH EPR spectra were observed, with their intensity decreasing over time until the  
578 end of the 30 min test. The integrated area of the EPR spectrum, which was proportional  
579 to the radical density,<sup>20</sup> was plotted as a function of time (Fig. 8d). Fuc-CMCS@Cur  
580 hydrogel beads without gastrointestinal digestion (incubated in PBS) showed a fast  
581 decline in DPPH EPR signals over time, with the signal reaching a steady state within  
582 approximately 10 min. This rapid radical-scavenging behavior was consistent with the  
583 well-recognized strong antioxidant activity of Cur. After digestion in SGF (2 h), the  
584 decay rate of the DPPH EPR signal slowed down noticeably. However, the overall  
585 percentage of EPR signal reduction within 30 min was only slightly affected, suggesting  
586 that the hydrogel matrix effectively shielded Cur from gastric stress and prevented  
587 substantial degradation. Following digestion in SIF (4 h), both the decay rate and the  
588 final intensity of the DPPH EPR signal were comparable to those of the undigested  
589 control in PBS, further confirming that Cur retained excellent antioxidant activity after  
590 intestinal digestion. Taken together, these results verified that Fuc-CMCS@Cur  
591 hydrogel beads preserved more than 90% of the antioxidant activity of Cur relative to



592 the undigested control (Table 1). The remarkable protective effect was attributed to the  
593 physical barrier formed by the polysaccharide network, which effectively insulated Cur  
594 from harsh digestive enzymes, acidic environments, and oxidative stress during  
595 gastrointestinal transit.



596 **Fig. 8.** EPR spectra of DPPH with Fuc-CMCS@Cur hydrogel beads after digestion in  
597 (a) PBS, (b) SGF, and (c) SIF, respectively; (d) time dependence of EPR signal  
598 reduction of DPPH with Fuc-CMCS@Cur hydrogel beads after digestion in PBS, SGF  
599 or SIF; (e) UV-vis spectra of the Fuc, CMCS, Cur, physical mixed solution of Fuc,  
600 CMCS and Cur, and disassembled solution of Fuc-CMCS@Cur; (f) FTIR spectra of  
601 the physical mixed solution of Fuc and CMCS, the physical mixed solution of Fuc,  
602 CMCS and Cur, and the disassembled solution of Fuc-CMCS@Cur.  
603

604  
605 Subsequently, the decay of the DPPH EPR signal over incubation time was fitted  
606 in an attempt to obtain quantitative results. The fitting parameters were presented in  
607 Table 1. The single exponential decay function was the best fit for the behavior of Fuc-  
608 CMCS@Cur treated in PBS and SIF, whereas the biexponential decay function was a



609 more accurate model for the response of Fuc-CMCS@Cur treated in SGF. This  
610 discrepancy suggested distinct mechanisms or processes for DPPH radical quenching.  
611 Complete release of Cur from Fuc-CMCS@Cur hydrogel beads was achieved in PBS  
612 or SIF, leading to homogeneous dispersion throughout the solution. All Cur was in a  
613 uniform chemical environment, ensuring equivalent accessibility to DPPH free radicals,  
614 thus exhibiting single exponential decay with no significant change in the primary time  
615 constant (designated as  $\tau_1$ ). In stark contrast, SGF treatment led to partial release  
616 characteristics, where only a minor fraction of Cur became freely dispersed in solution  
617 while the majority remained entrapped within the intact hydrogel matrix. This spatial  
618 confinement of hydrogel beads for incorporated Cur created differential accessibility  
619 for DPPH radicals and correspondingly distinct interaction kinetics between the free  
620 and encapsulated Cur fractions, ultimately manifesting as double exponential decay.  
621 The secondary time constant (designated as  $\tau_2$ ) exhibited a marked prolongation  
622 compared to  $\tau_1$ , attributable to the extended diffusion period required for DPPH radicals  
623 to permeate the dense polysaccharide-based hydrogel matrix prior to accessing  
624 encapsulated Cur molecules. Interestingly, the  $\tau_1$  value of Fuc-CMCS@Cur treated in  
625 SGF was significantly shorter than those in PBS and SIF. This phenomenon probably  
626 arose from the fact that Cur released in PBS or SIF continued to interact with the  
627 disassembled polysaccharide matrix of hydrogel beads, thereby impeding contact  
628 between DPPH free radicals and Cur. Conversely, the hydrogel beads maintained  
629 structural integrity in SGF, allowing the released Cur to remain freely dispersed in the  
630 solution, which facilitated immediate interaction with DPPH free radicals.



631 **Table 1.** Exponential fitting kinetic parameters of Fuc-CMCS@Cur hydrogel beads  
632 after digestion in various conditions determined by the EPR method.

Treatment	EPR signal reduction (%)	Maintained antioxidant capacity (%)	$\tau_1$ (min)	relative amplitude (%)	$\tau_2$ (min)	relative amplitude (%)	$R^2$ (%)
in PBS	71.39	100	2.65	100	0	0	99.73
in SGF 2 h	66.55	93.22	0.029	43.31	42.42	56.69	99.37
in SIF 4 h	68.09	95.38	2.75	100	0	0	99.92

633 Furthermore, to verify the above analysis, UV-vis and FTIR spectroscopy were  
634 employed to characterize the interaction between Cur and the disassembled hydrogel  
635 bead polysaccharide matrix. As attested in Fig. 8e, the UV-vis absorption of Cur in the  
636 disassembled solution of Fuc-CMCS@Cur hydrogel beads exhibited a red shift  
637 compared to free Cur. This finding confirmed the interaction between Cur and the  
638 polysaccharide matrix in solution, which was consistent with the physical mixed  
639 solution of Fuc, CMCS, and Cur (after excluding the UV-vis absorption interference of  
640 Fuc and CMCS). Meanwhile, as shown in the FTIR spectra of Fig. 8f, the broad peak  
641 that associated with the -OH stretching vibration in the physical mixed solution of Fuc  
642 and CMCS shifted from 3378 to 3337  $\text{cm}^{-1}$ , and the peak corresponding to C-O  
643 stretching vibration shifted from 1031 to 1059  $\text{cm}^{-1}$  upon the addition of Cur, as well  
644 as in the disassembled solution of Fuc-CMCS@Cur hydrogel beads. These shifts were  
645 attributed to hydrogen bonding interactions between Cur and polysaccharide matrix.<sup>43</sup>  
646 The findings confirmed the interaction between Cur and polysaccharide of the  
647 disassembled hydrogel beads, indicating that the polysaccharide matrix could protect  
648 Cur in the gastrointestinal environment to some extent even after the hydrogel beads



649 had disassembled in the intestine, thus ensuring sustained bioavailability.

#### 650 **4. Conclusions**

651 This study successfully fabricated pH-responsive polysaccharide hydrogel beads  
652 via physical crosslinking driven by hydrogen bonding between Fuc and CMCS, which  
653 constructed a stable three-dimensional network for Cur encapsulation. Cur served as  
654 both a bioactive agent and an additional crosslinker, enhancing the network  
655 crosslinking density and structural stability of the hydrogel. The hydrogel beads  
656 markedly improved the thermal stability and UV resistance of Cur, and exhibited  
657 favorable pH-responsive swelling and controlled release behavior. In simulated gastric  
658 fluid, the hydrogel beads maintained a compact structure with low Cur release, whereas  
659 nearly complete release was achieved in simulated intestinal fluid. Additionally, after  
660 *in vitro* simulated gastrointestinal digestion, the encapsulated Cur retained over 90% of  
661 its antioxidant activity, confirming the superior protective performance of the hydrogel  
662 beads. This green, food-grade delivery system provides an efficient and sustainable  
663 strategy for encapsulation and targeted delivery of labile polyphenolic compounds,  
664 addressing critical challenges in their stabilization and controlled release for  
665 nutraceutical and supplement applications.

666



667 **CRedit authorship contribution statement**

668 **Jiayu Yu:** Writing – original draft, Methodology, Investigation, Conceptualization.

669 **Hongyang Hu:** Validation, Investigation. **Yingyi Wang:** Validation, Investigation. **Xia**

670 **Sun:** Validation, Investigation. **Hanxu Li:** Validation, Investigation. **Shun Xiao:**

671 Validation, Investigation. **Bingcan Chen:** Writing – review & editing, Investigation,

672 Conceptualization. **Hui Li:** Writing – review & editing, Investigation, Funding

673 acquisition, Conceptualization.

674 **Declaration of competing interest**

675 The authors declare that they have no known competing financial interests or

676 personal relationships that could have appeared to influence the work reported in this

677 paper.

678 **Data availability**

679 Data will be made available on request.

680 **Acknowledgment**

681 This work was financially supported by the "Kuang Yaming-Tang Aoqing" Scholars

682 Talents Program from Jilin University (No. 419080524136). The Scientific and

683 Technological Project of Jilin Province of China (No. 20260205034GH). We appreciate

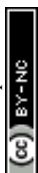
684 Prof. Yanxiong Pan for generously providing the EPR Instrument and helping with EPR

685 spectra acquisition and data analysis.

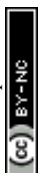
686 **References**

687 1. Z. Rafiee, M. Nejatian, M. Daeihamed and S. M. Jafari, Application of different

688 nanocarriers for encapsulation of curcumin, *Crit. Rev. Food Sci. Nutr.*, 2019,



- 689           **59**, 3468-3497.
- 690    2.    Q. B. Hu and Y. C. Luo, Chitosan-based nanocarriers for encapsulation and  
691    delivery of curcumin: A review, *Int. J. Biol. Macromol.*, 2021, **179**, 125-135.
- 692    3.    L. Q. Zou, B. J. Zheng, R. J. Zhang, Z. P. Zhang, W. Liu, C. M. Liu, H. Xiao  
693    and D. J. McClements, Food-grade nanoparticles for encapsulation, protection  
694    and delivery of curcumin: comparison of lipid, protein, and phospholipid  
695    nanoparticles under simulated gastrointestinal conditions, *RSC Adv.*, 2016, **6**,  
696    3126-3136.
- 697    4.    G. Y. Kan, L. J. Chen, W. J. Zhang, Q. Q. Bian, X. C. Wang and J. Zhong,  
698    Recent advances in the development and application of curcumin-loaded  
699    micro/nanocarriers in food research, *Adv. Colloid Interface Sci.*, 2025, **335**,  
700    103333.
- 701    5.    M. Zhou, F. L. Li, J. Chen, Q. S. Wu and Z. Y. Zou, Research progress on  
702    natural bio-based encapsulation system of curcumin and its stabilization  
703    mechanism, *Food Sci. Technol.*, 2022, **42**, e78422.
- 704    6.    T. Thambi, V. H. G. Phan and D. S. Lee, Stimuli-sensitive injectable hydrogels  
705    based on polysaccharides and their biomedical applications, *Macromol. Rapid*  
706    *Commun.*, 2016, **37**, 1881-1896.
- 707    7.    L. Liu, Y. Zhang, S. Yu, Z. Yang, C. He and X. Chen, Dual stimuli-responsive  
708    nanoparticle-incorporated hydrogels as an oral insulin carrier for intestine-  
709    targeted delivery and enhanced paracellular permeation, *ACS Biomater. Sci.*  
710    *Eng.*, 2018, **4**, 2889-2902.



- 711 8. J. H. Fitton, D. N. Stringer, A. Y. Park and S. S. Karpinić, Therapies from  
712 fucoidan: New developments, *Mar. Drugs*, 2019, **17**, 571.
- 713 9. S. M. Etman, Y. S. R. Elnaggar and O. Y. Abdallah, "Fucoidan, a natural  
714 biopolymer in cancer combating: From edible algae to nanocarrier tailoring",  
715 *Int. J. Biol. Macromol.*, 2020, **147**, 799-808.
- 716 10. Y.-C. Huang, J.-K. Chen, U. I. Lam and S.-Y. Chen, Preparing, characterizing,  
717 and evaluating chitosan/fucoidan nanoparticles as oral delivery carriers, *J.*  
718 *Polym. Res.*, 2014, **21**, 415.
- 719 11. G. Zhai, Y. Wang, P. Han, T. Xiao, J. You, C. Guo and X. Wu, Drug loaded  
720 marine polysaccharides-based hydrogel dressings for treating skin burns, *Int. J.*  
721 *Biol. Macromol.*, 2024, **281**, 135779.
- 722 12. X. Lv, W. Zhang, Y. Liu, Y. Zhao, J. Zhang and M. Hou, Hygroscopicity  
723 modulation of hydrogels based on carboxymethyl chitosan/alginate  
724 polyelectrolyte complexes and its application as pH-sensitive delivery system,  
725 *Carbohydr. Polym.*, 2018, **198**, 86-93.
- 726 13. N. Wang, J. Tian, L. Wang, S. Song, C. Ai, S. Janaswamy and C. Wen, Fucoidan  
727 hydrogels induced by k-carrageenan: Rheological, thermal and structural  
728 characterization, *Int. J. Biol. Macromol.*, 2021, **191**, 514-520.
- 729 14. R. Chang, D. Zhao, C. Zhang, K. Liu, Y. He, F. Guan and M. Yao, PMN-  
730 incorporated multifunctional chitosan hydrogel for postoperative synergistic  
731 photothermal melanoma therapy and skin regeneration, *Int. J. Biol. Macromol.*,  
732 2023, **253**, 126854.



- 733 15. H.-T. Lu, T.-W. Lu, C.-H. Chen, K.-Y. Lu and F.-L. Mi, Development of  
734 nanocomposite scaffolds based on biomineralization of carboxymethyl  
735 chitosan/fucoidan conjugates for bone tissue engineering, *Int. J. Biol.*  
736 *Macromol.*, 2018, **120**, 2335-2345.
- 737 16. H.-Y. Tang, Z. Fang and K. Ng, Dietary fiber-based colon-targeted delivery  
738 systems for polyphenols, *Trends Food Sci. Technol.*, 2020, **100**, 333-348.
- 739 17. M. Baharizade, S. I. Ghetmiri, M. Mohammady, S. Mohammadi-Samani and G.  
740 Yousefi, Revolutionizing knee osteoarthritis treatment: Innovative self-nano-  
741 emulsifying polyethylene glycol organogel of curcumin for effective topical  
742 delivery, *Aaps Pharmscitech*, 2024, **25**, 80.
- 743 18. N. Yuan, L. Xu, H. Wang, Y. Fu, Z. Zhang, L. Liu, C. Wang, J. Zhao and J.  
744 Rong, Dual Physically Cross-Linked Double Network Hydrogels with High  
745 Mechanical Strength, Fatigue Resistance, Notch-Insensitivity, and Self-Healing  
746 Properties, *ACS Appl. Mater. Interfaces*, 2016, **8**, 34034-34044.
- 747 19. X. Huang, J. Wang, R. Liu, C. Yang, Y. Shao, X. Wang, H. Yi and Y. Lu, An  
748 effective potential bifidobacterium animalis F1-7 delivery strategy:  
749 Supramolecular hydrogel - sodium alginate/ tryptophan-sulfobutylether- $\beta$ -  
750 cyclodextrin (Alg/Trp-SBE- $\beta$ -CD), *Food Hydrocoll.*, 2024, **155**, 110217.
- 751 20. H. Li, Y. Pan, Z. Yang, J. Rao and B. Chen, Improving antioxidant activity of  
752  $\beta$ -Lactoglobulin by nature-inspired Cconjugation with gentisic acid, *J. Agric.*  
753 *Food Chem.*, 2019, **67**, 11741-11751.
- 754 21. J. H. Muyonga, C. G. B. Cole and K. G. Duodu, Characterisation of acid soluble



- 755 collagen from skins of young and adult Nile perch (*Lates niloticus*), *Food Chem.*,  
756 2004, **85**, 81-89.
- 757 22. P. S. Saravana, S. Karuppusamy, D. K. Rai, J. Wanigasekara, J. Curtin and B.  
758 K. Tiwari, Elimination of ethanol for the production of fucoidans from brown  
759 seaweeds: Characterization and bioactivities, *Mar. Drugs*, 2024, **22**, 493.
- 760 23. J. Ge, P. Yue, J. Chi, J. Liang and X. Gao, Formation and stability of  
761 anthocyanins-loaded nanocomplexes prepared with chitosan hydrochloride and  
762 carboxymethyl chitosan, *Food Hydrocoll.*, 2018, **74**, 23-31.
- 763 24. Y. Zhang, W. Zhao, Z. Lin, Z. Tang and B. Lin, Carboxymethyl  
764 chitosan/sodium alginate hydrogel films with good biocompatibility and  
765 reproducibility by in situ ultra-fast crosslinking for efficient preservation of  
766 strawberry, *Carbohydr. Polym.*, 2023, **316**, 121073.
- 767 25. Y. H. Lin, H. F. Liang, C. K. Chung, M. C. Chen and H. W. Sung, Physically  
768 crosslinked alginate/N,O-carboxymethyl chitosan hydrogels with calcium for  
769 oral delivery of protein drugs, *Biomaterials*, 2005, **26**, 2105-2113.
- 770 26. M.-C. Lee and Y.-C. Huang, Soluble eggshell membrane protein-loaded  
771 chitosan/fucoidan nanoparticles for treatment of defective intestinal epithelial  
772 cells, *Int. J. Biol. Macromol.*, 2019, **131**, 949-958.
- 773 27. V. K. Pawar, Y. Singh, K. Sharma, A. Shrivastav, A. Sharma, A. Singh, J. G.  
774 Meher, P. Singh, K. Raval, A. Kumar, H. K. Bora, D. Datta, J. Lal and M. K.  
775 Chourasia, Improved chemotherapy against breast cancer through  
776 immunotherapeutic activity of fucoidan decorated electrostatically assembled



- 777 nanoparticles bearing doxorubicin, *Int. J. Biol. Macromol.*, 2019, **122**, 1100-  
778 1114.
- 779 28. G. Huang, Y. Yan, D. Xu, J. Wu, C. Xu, L. Fu and B. Lin, Curcumin-loaded  
780 nanoMOFs@CMFP: A biological preserving paste with antibacterial properties  
781 and long-acting, controllable release, *Food Chem.*, 2021, **337**, 127987.
- 782 29. M. Mohammadian, M. Salami, S. Momen, F. Alavi and Z. Emam-Djomeh,  
783 Fabrication of curcumin-loaded whey protein microgels: Structural properties,  
784 antioxidant activity, and in vitro release behavior, *LWT-Food Sci. Technol.*,  
785 2019, **103**, 94-100.
- 786 30. R. Priyadarshi, Z. Riahi and J.-W. Rhim, Antioxidant pectin/pullulan edible  
787 coating incorporated with *Vitis vinifera* grape seed extract for extending the  
788 shelf life of peanuts, *Postharvest Biol. Technol.*, 2022, **183**, 111740.
- 789 31. K. Liu, X.-Q. Zha, W.-D. Shen, Q.-M. Li, L.-H. Pan and J.-P. Luo, The hydrogel  
790 of whey protein isolate coated by lotus root amylopectin enhance the stability  
791 and bioavailability of quercetin, *Carbohydr. Polym.*, 2020, **236**, 116009.
- 792 32. P. Wang, Z.-g. Luo and Z.-g. Xiao, Preparation, physicochemical  
793 characterization and in vitro release behavior of resveratrol-loaded oxidized  
794 gellan gum/resistant starch hydrogel beads, *Carbohydr. Polym.*, 2021, **260**,  
795 117794.
- 796 33. X. Huang, X. Kou, L. Wang, R. Ji, C. Ma and H. Wang, Effective hydroxylation  
797 of tangeretin from Citrus Peel (Chenpi) by edible acids and its improvement in  
798 antioxidant and anti-lipase activities, *LWT-Food Sci. Technol.*, 2019, **116**,



- 799 108469.
- 800 34. X. Chen, H. Liu, Y. Yang, P. Li, X. Wang, K. Zhang, K. Zeng, J. Ming and X.  
801 Lei, Chitosan-based emulsion gel beads developed on the multiple-unit floating  
802 delivery system for gastric sustained release of proanthocyanidins, *Food*  
803 *Hydrocoll.*, 2025, **159**, 110704.
- 804 35. H. Jing, X. Huang, X. Du, L. Mo, C. Ma and H. Wang, Facile synthesis of pH-  
805 responsive sodium alginate/carboxymethyl chitosan hydrogel beads promoted  
806 by hydrogen bond, *Carbohydr. Polym.*, 2022, **278**, 118993.
- 807 36. L. Cao, D. Van de Walle, H. Hirmz, E. Wynendaele, K. Dewettinck, B. V.  
808 Parakhonskiy and A. G. Skirtach, Food-based biomaterials: pH-responsive  
809 alginate/gellan gum/carboxymethyl cellulose hydrogel beads for lactoferrin  
810 delivery, *Biomater. Adv.*, 2024, **165**, 213999.
- 811 37. Y. Yang, Y. Liu, S. Chen, K.-L. Cheong and B. Teng, Carboxymethyl  $\beta$ -  
812 cyclodextrin grafted carboxymethyl chitosan hydrogel-based microparticles for  
813 oral insulin delivery, *Carbohydr. Polym.*, 2020, **246**, 116617.
- 814 38. H. Bi, X. Zhang, Q. Wang, Q. Yong, W. Xu, M. Xu, C. Xu and X. Wang,  
815 Dynamic reversible disulfide bonds hydrogel of thiolated  
816 galactoglucomannan/cellulose nanofibril with self-healing property for protein  
817 release, *Ind. Crops Prod.*, 2023, **206**, 117615.
- 818 39. C. Zhu, X. Zhang, J. Gan, D. Geng, X. Bian, Y. Cheng and N. Tang, A pH-  
819 sensitive hydrogel based on carboxymethylated konjac glucomannan  
820 crosslinked by sodium trimetaphosphate: Synthesis, characterization, swelling



- 821 behavior and controlled drug release, *Int. J. Biol. Macromol.*, 2023, **232**, 123392.
- 822 40. J. Adiwidjaja, A. J. McLachlan and A. V. Boddy, Curcumin as a clinically-  
823 promising anti-cancer agent: pharmacokinetics and drug interactions, *Expert*  
824 *Opinion on Drug Metabolism & Toxicology*, 2017, **13**, 953-972.
- 825 41. D. Sanna, G. Delogu, M. Mulas, M. Schirra and A. Fadda, Determination of  
826 free radical scavenging activity of plant extracts through DPPH assay: An EPR  
827 and UV-Vis study, *Food Anal. Method.*, 2012, **5**, 759-766.
- 828 42. M. Polovka, V. Brezová and A. Stasko, Antioxidant properties of tea  
829 investigated by EPR spectroscopy, *Biophys. Chem.*, 2003, **106**, 39-56.
- 830 43. Y. Zhang, D. Guo, X. Shen, Z. Tang and B. Lin, Recoverable and degradable  
831 carboxymethyl chitosan polyelectrolyte hydrogel film for ultra stable  
832 encapsulation of curcumin, *Int. J. Biol. Macromol.*, 2024, **268**, 131616.
- 833
- 834

